Simulation of the scrape-off layer plasma during a disruption

T.D. Rognlien [a,*], J.A. Crotinger [a], G.D. Porter [a], G.R. Smith [a], A.G. Kellman [b], P.L. Taylor [b]

[a] *Lawrence Livermore National Laboratory, Livermore, CA 94551, USA*
[b] *General Atomics, San Diego, CA 92186, USA*

Abstract

The evolution of the scrape-off layer (SOL) during a disruption in the DIII-D tokamak is modeled using the 2-D UEDGE transport code. The focus is on the thermal quench phase when most of the energy content of the discharge is rapidly transported across the magnetic separatrix where it then flows to material surfaces or is radiated. Comparisons between the simulation and an experiment on the DIII-D tokamak are made with the heat flux to the divertor plate, and temperature and density profiles at the SOL midplane. The temporal response of the heat flux to the divertor plate is calculated. The sensitivity of the solution to assumptions of electron heat-flux models and impurity radiation is investigated.

Keywords: SOL plasma; Divertor plasma; DIII-D; Fluid simulation; Disruptions

1. Introduction

Disruptions in tokamaks can often be characterized by two periods: the first is the thermal quench where the plasma energy of the core is lost, and the second is the current decay where the plasma current is lost [1]. The scrape-off layer (SOL) plasma takes on an important role during the thermal quench of a tokamak disruption. Specifically, the SOL properties determine how the power from the core plasma is distributed on material surfaces, how impurities radiation affects the power loss, and how plasma current reaches the vessel wall to initiate halo currents. The location and temporal variation of the heat load on surfaces are important input for material ablation calculations [2]. In addition to the large heat fluxes, the plasma current is typically shunted through the vacuum vessel in the current-decay phase, causing large $\mathbf{J} \times \mathbf{B}$ forces on the vessel. Also, the large inductive electric field during current-decay phase can produce damaging run-away electrons. All of these consequences of disruptions are of concern for large future devices such as ITER.

In an effort to better understand the energy loss during the thermal quench, we simulate the SOL plasma for the DIII-D tokamak [3,4] using the time-dependent transport code UEDGE [6,7]. Our primary focus here is on the initial thermal quench phase when most of the core energy is lost, but the total current and the shape of the MHD equilibrium is maintained. In Section 2, we describe the experimentally measured characteristics of a disruption in DIII-D, and the simulation model is described in Section 3. Section 4 contains a comparison between the experiment and the simulation where we discussion the importance of assumptions in the model, and we give a summary in Section 4.

2. Experimental measurements during a disruption

Various types of disruptions can occur in the DIII-D tokamak, e.g., from puffing deuterium or impurity gas and from exceeding a plasma β-limit. Impurity induced disruptions in DIII-D are described elsewhere [3,4]. Here we consider a β-limit disruption that occurred on discharge 84539. This single-null divertor discharge had a plasma current of 1.5 MA, a toroidal magnetic field of 1.2 T, and a q safety factor of ~ 2.5. The plasma shape is defined by the outer magnetic flux surfaces constructed by the EFITD code [5] shown in Fig. 1; also shown is the corresponding

* Corresponding author. Tel: +1-510 422 9830; fax: +1-510 423 3484; e-mail: rognlien@llnl.gov.
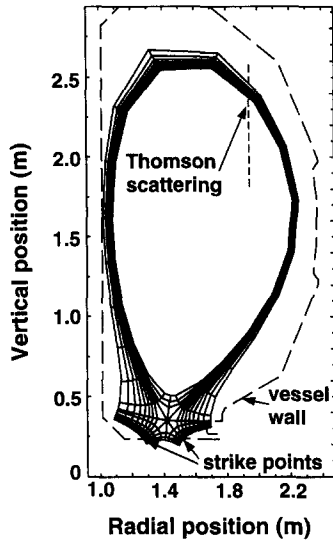
Fig. 1. Outer magnetic flux surfaces for DIII-D discharge 84359 at $t = 2.20$ s showing typical orthogonal mesh used in the UEDGE simulation.

UEDGE 2-D orthogonal mesh which uses the flux surfaces as one coordinate. Neutral beam injection was ramped up to 17 MW before the disruption near 2.2 s into the discharge. In Fig. 2, we show the plasma current I_p) and the central soft X-ray signal ($\propto$ central electron temperature, T_{ec}) near the time of the disruption. First, the plasma energy in the core decays (measured by T_{ec}), followed by the decay of I_p.

During the time of the thermal quench (2.20 to 2.21 s), the heat flux on the divertor plates measured by the infrared camera system (IRTV) rises rapidly and broadens as shown in Fig. 3. The inner and outer plate separatrix strike points are denoted by the dashed lines on the major axis coordinate, R (see Fig. 1). Note that the heat flux is predominantly on the SOL sides of the strike points. Also, often the temporal behavior is characterized by bursts with
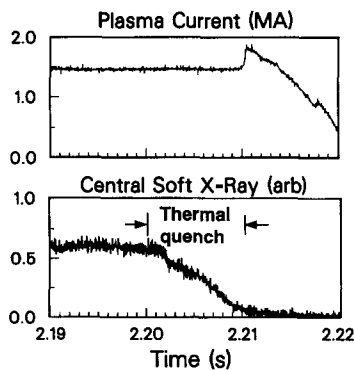

Fig. 2. Variation of plasma current and central soft X-ray signal proportional to T_{ec} for DIII-D discharge 84359.
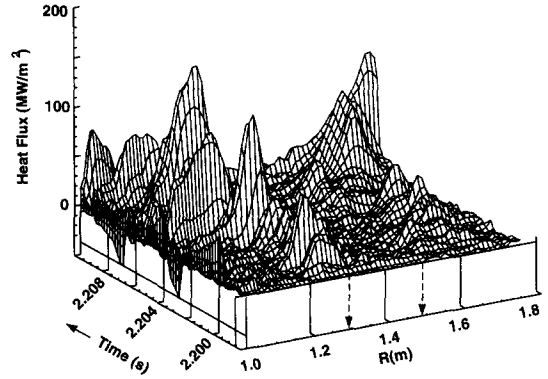

Fig. 3. Temporal and spatial variation of divertor plate heat flux as measured by the infrared camera system (IRTV) for discharge 84359. The dashed lines denote the approximate location of the inner and outer separatrix strike points.

widths of 0.5–1 ms, which is about the temporal resolution of the IRTV.

The electron temperature (T_e) and density (n) are measured by a Thomson scattering system near the outer midplane. Three time slices are shown in Fig. 4, the first being before the disruption, the second is half-way through the thermal quench and the last is at the end of the thermal quench. Note the broadening of the SOL and the decrease in the temperature deeper into the core. Because of the scale, the first two time slices do not show the maximum T_e measured (near $r/a = 0.4$): at $t = 2.1860$ s, $T_{e\text{-max}} \approx 1.5$ keV and at $t = 2.2055$ s, $T_{e\text{-max}} \approx 1.0$ keV. There are charge-exchange recombination (CER) measurements of the ion temperature, T_i, which is typically a factor of two or more above T_e.
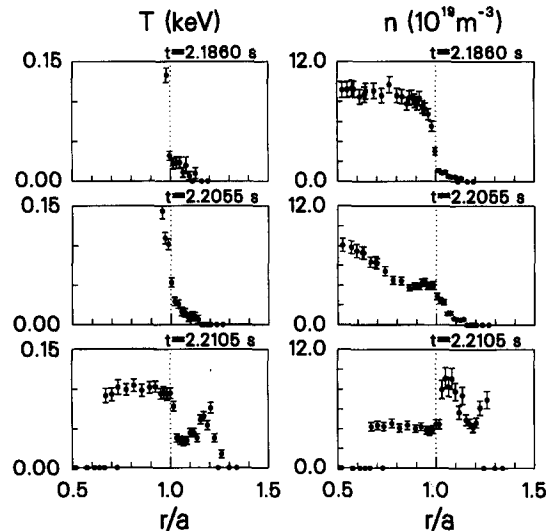

Fig. 4. Electron temperature (T) and density (n) near the edge region of the midplane as measured by Thomson scattering at various times.

3. Numerical model

The UEDGE code solves for the plasma fluid equations in the 2-D poloidal plane, including the region somewhat inside the separatrix and extending into the SOL. A finite volume discretization method is used, and the resulting difference equations are solved with a fully implicit Newton method [6,7]. The code has been used in a steady-state mode to model many normal (non-disrupting) DIII-D discharges [10]. The 2-D orthogonal flux-surface mesh is shown in Fig. 1; increasing the mesh beyond the 34×18 shown has little effect on the results. With the poloidal flux, ψ, normalized to unity on the separatrix, we take the inner simulation boundary to be $\psi_c = 0.98$ and the outer boundary at $\psi_w = 1.10$.

Plasma equations are solved for the ion density, n_i, and ion parallel velocity $v_{i\parallel}$ and separate equations are used for the electron and ion temperatures, T_e and T_i. Poloidal transport is the geometrical projection of the parallel transport from Braginskii [8], except that thermal flux limits are used as discussed below. Radial transport is described by anomalous diffusion coefficients chosen to fit experimental data. We can use separate diffusion coefficients for density (D), electron energy (χ_e) and ion energy (χ_i). The neutral species is modeled by a simple 2-D diffusive fluid equation for the present calculations. Atomic physics rate coefficients for ionization, recombination, and the associated energy loss are provided by look-up tables as described elsewhere [9].

The practice of adjusting the radial diffusion coefficients to obtain a fit to experimental data requires some comment for the case of disruptions where the details of the transport are not well understood and may not even be diffusive. However, given that the plasma energy is somehow transported to open magnetic field lines in the thermal quench time, we can study the 2-D effect of the competition between the radial flux and the assumed classical parallel transport to see if a consistent picture evolves.

One correction to the classical parallel transport that we consider is limiting the thermal heat flux. With the diffusive thermal fluxes being $q_{e,i} = -\kappa_{e,i} \partial T_{e,i}/\partial s$, the modification is as follows

$$\kappa_{e,i} \rightarrow \frac{\kappa_{e,i}}{(1 + |q_{e,i}|/q_f)}. \tag{1}$$

Here $q_f = c_f n v_{te,ti} T_{e,i}$ is the thermal flux reduced by the coefficient c_f. More discussion of flux limiting for normal discharge parameters is given elsewhere [11]. However, for disruptions, little is know of the particle distribution functions. Therefore, we shall treat c_f unknown, and investigate the effect of taking different values.

4. Simulation of the SOL and comparison with the experiment

We obtain a pre-disruption equilibrium with UEDGE by using the anomalous diffusion coefficients of $D = \chi_e =$

$\chi_i = 1$ m^2/s. While these give fair comparison with the data, no attempt was made to fit the pre-disruption data precisely as we focus on the disruption period. The recycling coefficient at the plates are set at 0.95 throughout the simulations. As can be seen from Fig. 2, the energy of the plasma is lost in a time of about 10 ms and the energy striking the plates in this time is ~ 1 MJ. Allowing for a 50% duty factor for the load on the plates (see Fig. 3), we translate this into a boundary condition at the core edge for UEDGE of 1 MJ/(0.5 $\times$ 10 ms) $=$ 200 MW, which we divide equally between the ions and electrons. With this boundary condition, UEDGE evolves the SOL plasma to equilibrium.

We have run a number of simulations with different spatially constant anomalous diffusion coefficients to fit the shape of the divertor heat-flux profiles shown in Fig. 3 and find that a reasonable fit is found for $D = \chi_e = \chi_i = 20$ m^2/s. The temporal evolution of the heat-flux profiles on the inner and outer divertor plates is shown in Fig. 5. The five rising curves correspond in order to increasing times from the initiation of the disruption (see caption). Thus, the increased heat flux first arrives at the outer plate, it being closer to the outer midplane where a majority of the power is injected into the SOL owing to the more compressed flux surfaces there. The flux on both plates is close to steady-state by $t = 0.3$ ms, and the total power to each plate is nearly the same. The time scale and shape are consistent with the experimental profiles shown in Fig. 3. There is even a suggestion of the heat pulses being narrower and more peaked on the inner plate, but the data is too varied for a clear conclusion. The inner/outer asymmetries may also have to do with toroidal variations that we do not consider. We did include parallel electric currents from electrostatic fields which lead to small changes
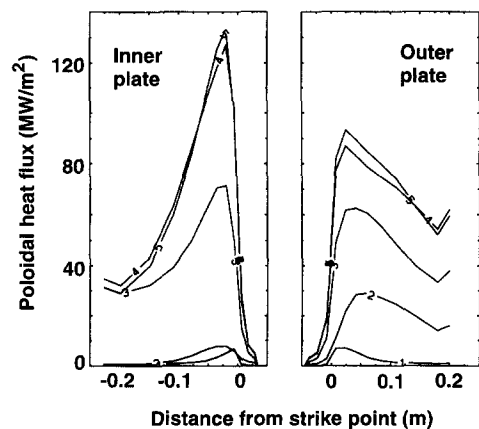

Fig. 5. Time history of heat flux on the inner and outer divertor plates from UEDGE with $D = \chi_e = \chi_i = 20$ m^2/s. The five curves with increasing heat flux correspond respectively to the post-disruption times 0 s, 0.03 ms, 0.1 ms, 0.3 ms, and steady-state. Distance is measured normal to flux surfaces.

in the asymmetry for the disruption period, but do enhance the outer plate power by 30% for the pre-disruption equilibrium. We plan to extend this to inductive fields.

The total heat-flux profiles are not too sensitive to the choice of the flux-limit factors, c_f, for the electrons and ions; the results in Fig. 5 has $c_{fe} = 0.1$ for electrons and $c_{fi} \rightarrow \infty$ for ions. The plate temperatures do decrease with c_f somewhat, but the midplane values where we have the Thomson data are not strongly affected. The peak plate T_e is about 250 eV without flux limiting and 200 eV with $c_{fe} = 0.1$. An enhanced energy transmission factor from kinetic effects decreases the plate temperatures; here we have used standard values of 4.0 for electrons and 2.5 for ions. Another effect reducing T_e at the plate is impurity radiation.

Bolometer measurements indicate that ~ 30–40% of the energy is radiated during the disruption. We have modeled this by using a fixed fraction, coronal equilibrium model of carbon impurities corresponding to a well-mixed plasma. While no impurities were injected for this discharge, carbon is used account for erosion from the carbon divertor plates and walls. In order to get ~ 30% of the power radiated, we need a carbon fraction of 25%. The radiation occurs close to the divertor plates, but peaks about 6 cm away from the separatrix where the plate T_e is reduced to ~ 10 eV; in this case, the peak plate T_e is reduced to 100 eV. The effect on the plasma heat-flux profile is shown in Fig. 6; the absorption of the impurity radiation on the plate is not included, but would broaden the profile modestly. In the current decay phase, it will be important to evolve the impurity species [1].

Direct comparison between midplane experimental data of T_e and T_i and the simulation with 25% carbon is shown in Fig. 7. The dotted line for T_i for $\delta R = R - R_{sep} < 0$ does connect to a data point not shown. The comparison would fit better if the separatrix position were moved
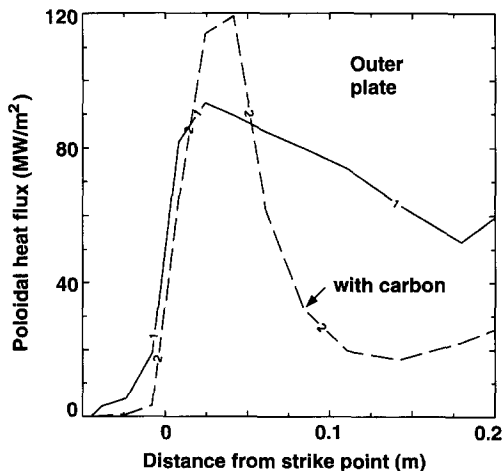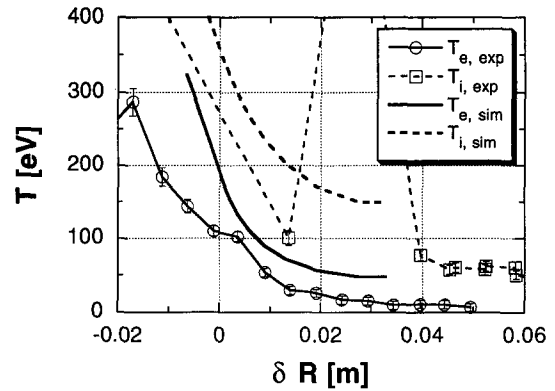

Fig. 7. Comparison of T_e (Thomson scattering) and T_i (CER) at the midplane for $t = 2205$ s (lines with data points) with the UEDGE simulation (lines without data points).

about 1 cm, shifting the experimental data outward. Such a shift is within typical error range caused by the uncertainty in the data for the EFITD analysis. The data channel corresponding to the high experimental T_i at $\delta R = 2.6$ cm appears abnormally high on many time slices with different δR, and may have been malfunctioning. The experimental density (not shown) decays a factor of two over the simulation region while the simulation density only decays about 20%. The differences between the simulation and experimental profiles may indicate the limitation of the diffusive model. The effect of removing the impurity radiation is to increase the midplane simulation temperatures by 30–40% in the SOL region.

5. Summary

We have simulated the thermal quench phase of a high β-disruption in DIII-D using the UEDGE transport code. Choosing anomalous diffusion coefficients of 20 m²/s gives a reasonable fit to the divertor heat-flux profiles. The response time of ~ 0.3 ms is roughly consistent with the data. Kinetic effects such as thermal flux limits and enhance energy transmission primarily affect the temperatures on the plates, and not the heat-flux profiles. Impurity radiation also reduces the plate T_e and narrows the heat-flux profile. Rough agreement is found for the midplane temperature profiles and shifting the separatrix 1 cm would improve this.

These calculations show the feasibility of modeling a number of the SOL aspects of disruptions with a transport code that could be used in ablation studies; the detailed nature of the escaping energy spectrum requires a kinetic treatment. Important additional work to be done is to assess the response of the growing SOL to carrying current induced by the rising loop voltage and to couple the core and edge regions together using our CORSICA-2 code.

Fig. 6. Plasma heat flux on outer plate with and without 25% fixed-fraction of carbon.

References

[1] D.J. Ward and J.A. Wesson, Nucl. Fusion 32 (1992) 1117.
[2] A.E. Koniges et al., these Proceedings, p. 244.
[3] P.L. Taylor, A.G. Kellman, B.W. Rice and D.A. Humphreys, Phys. Rev. Lett. 76 (1996) 916.
[4] P.L. Taylor et al., in: Proc. 22th EPS Conf. Contr. Fusion Plasma Phys., Bournemouth, 1995, Part IV, p. 49.
[5] L.L. Lao et al., Nucl. Fusion 30 (1990) 1035.
[6] T.D. Rognlien et al., Contr. Plasma Phys. 34 (1994) 362.
[7] G.R. Smith, P.N. Brown, R.B. Campbell, D.A. Knoll, P.R. McHugh, M.E. Rensink and T.D. Rognlien, J. Nucl. Mat. 220–222 (1995) 1024.
[8] 5.1. Braginskii, in: Transport Processes in a Plasma, Reviews of Plasma Physics, Vol. 1, ed. M.A. Leontovich (Consultants Bureau, New York, 1965) p. 205.
[9] T.D. Rognlien, B.J. Braams and D.A. Knoll, Contrib. Plasma Phys., 36 (1996) 105.
[10] G.D. Porter et al., Phys. Plasmas 3 (1996) 1967.
[11] R.H. Cohen and T.D. Rognlien, Contrib. Plasma Phys. 34 (1994) 198.